J. Biochem. 2011;150(1):39–47 doi:10.1093/jb/mvr034

JB THE JOURNAL OF BIOCHEMISTRY

The effects of an ideal β-turn on β-2 microglobulin fold stability

Received January 14, 2011; accepted February 27, 2011; published online March 11, 2011

Matteo Colombo[1], Stefano Ricagno[1], Alberto Barbiroli[2], Carlo Santambrogio[3], Sofia Giorgetti[4,5], Sara Raimondi[4,5], Francesco Bonomi[2], Rita Grandori[3], Vittorio Bellotti[4,5] and Martino Bolognesi[1,*]

[1]Dipartimento di Scienze Biomolecolari e Biotecnologie, CNR-INFM and CIMAINA, Università di Milano, Via Celoria 26, 20133 Milan, Italy; [2]Dipartimento di Scienze Molecolari Agroalimentari, Sezione di Biochimica, Università di Milano, Via Celoria 2, 20133 Milan, Italy; [3]Dipartimento di Biotecnologie e Bioscienze, Università di Milano-Bicocca, Piazza della Scienza 2, 20126 Milan, Italy; [4]Dipartimento di Biochimica, Università di Pavia, Via Taramelli 3/b, 27100 Pavia, Italy; and [5]Laboratori di Biotecnologie IRCCS Fondazione Policlinico San Matteo, Pavia, Italy

*Martino Bolognesi, Department of Biomolecular Sciences & Biotechnology, University of Milano, Via Celoria, 26, I-20133 Milano, Italy. Tel: +39 02 50314893, Fax: +39 02 50314895, email: martino.bolognesi@unimi.it

Accession numbers: K58P-W60G β2m atomic coordinates and structure factors were deposited in the Protein Data Bank (code 3IB4).

Beta-2 microglobulin (β2m) is the light chain of Class I major histocompatibility complex (MHC-I) complex. β2m is an intrinsically amyloidogenic protein capable of forming amyloid fibrils *in vitro* and *in vivo*. β2m displays the typical immunoglobulin-like fold with a disulphide bridge (Cys25–Cys80) cross-linking the two β-sheets. Engineering of the loop comprised between β-strands D and E has shown that mutations in this region affect protein structure, fold stability, folding kinetics and amyloid aggregation properties. Such overall effects have been related to the DE loop backbone structure, which presents a strained conformation in the wild-type (wt) protein, and a type I β-turn in the W60G mutant. Here, we report a biophysical and structural characterization of the K58P-W60G β2m mutant, where a Pro residue has been introduced in the type I β-turn $i+1$ position. The K58P-W60G mutant shows improved chemical and temperature stability and faster folding relative to wt β2m. The crystal structure (1.25 Å resolution) shows that the Cys25–Cys80 disulphide bridge is unexpectedly severed, in agreement with electrospray ionization–mass spectrometry (ESI–MS) spectra that indicate that a fraction of the purified protein lacks the internal disulphide bond. These observations suggest a stabilizing role for Pro58, and stress a crucial role for the DE loop in determining β2m biophysical properties.

Keywords: Beta-2-microglobulin/dialysis-related amyloidosis/fold stability/crystal structure/disulphide bond.

Abbreviations: β2m, β2 microglobulin; CD, circular dichroism; C_m, melting concentration; CR, Congo Red; CSD, charge-state distribution; DTT, dithiothreitol; DTNB, 5,5′-dithiobis-(2-nitrobenzoic acid); DRA, dialysis-related amyloidosis; ESI–MS, electrospray ionization–mass spectrometry; K58P-W60G, β2 microglobulin Asp58→Pro58 and Trp60→Gly60 double mutant; MHC-I, Class I major histocompatibility complex; SDS, sodium dodecyl sulphate; T_m, melting temperature; TFE, trifluoroethanol; ThT, Thioflavin T; wt, wild-type.

Amyloidosis, the *in vivo* deposition of protein fibril material, is linked to specific protein misfolding diseases, often leading to neurodegeneration, such as Alzheimer disease in man and spongiform encephalopathy in cow (*1*). Formation of amyloid plaques arises from the aggregation of partially or totally unfolded protein molecules into elongated protein fibrils, known as amyloid fibrils, characterized by a typical cross-β structure (*2*), and by high mechanical and chemical resistance (*1*). Among recognized amyloidogenic proteins, β-2 microglobulin (β2m) has been considered and used as a model for studies on folding, aggregation and amyloid fibril formation (*3*), being directly responsible for the disease known as dialysis-related amyloidosis (DRA). β2m is the light chain of Class I major histocompatibility complex (MHC-I) and CD1 (*4*). β2m is a 99 residues protein endowed with a typical immunoglobulin fold, where two facing β-sheets, one containing strands ABDE and the other containing strands CFG, are linked by a core disulphide bond between Cys-25 (strand B) and Cys-80 (strand F). Under physiological conditions, β2m dissociated from MHC-I heavy chain is released in serum and transported to the kidneys where it is degraded. In patients with renal failure, β2m cannot be removed from blood circulation and its concentration increases up to 50-fold (*5*). When such high concentration level is retained for years, β2m aggregates into amyloid fibrils, leading to DRA (*6*). β2m fibrils can also be formed *in vitro* under chemically controlled conditions, such as acidic pH (2.5), or neutral pH in the presence of trifluoroethanol (TFE) or sodium dodecyl sulphate (SDS) (*7*).

Although a general mechanism of amyloid fibril formation has not yet been completely defined for β2m, some specific regions of the molecule have been shown to be critical for aggregation. The analysis of amyloid plaques extracted from DRA patients has shown the presence of the ΔN6 β2m variant, which is characterized by the absence of the N-terminal hexapeptide (*8*). Recently, a P5G mutant has been shown

to be prone to aggregation similarly to ΔN6 β2m (*9*). Furthermore, an important role has been assessed for the β2m Pro32 residue that shows a *cis*-peptide bond in wild-type (wt) β2m. In the P32A β2m mutant, the amide group of Ala32, has a *trans* conformation, determining a total abrogation of the lag phase observed for the formation of amyloid fibrils in the wt protein (*10*). It has also been reported that, under acidic conditions, substitution of the aromatic residues in the 62–70 sequence stretch with Ala, results in a decreased fibril elongation rate and an increased fibrillogenesis lag time (*11*), suggesting that this hydrophobic region is important for the fibril nucleation mechanism.

The aggregation properties of wt and mutant β2m have also been investigated by electrospray ionization–mass spectrometry (ESI–MS) and ion mobility. Three species of β2m have been identified (native, partially unfolded and acid unfolded), whose distribution depends on pH and mutations (*12–15*). Recently, the β2m loop between the D and E strands, which comprises residues 57–60, has been shown to be critical for β2m amyloid propensity (*16*). In particular, Trp60 is a strongly conserved residue among vertebrates due to its crucial role in the association of β2m with the heavy chain in the MHC-I complex (*16*). The substitution of the conserved residue Trp60 with Gly totally abrogates the amyloidogenic process under mild conditions, and results in an increased fold stability compared to wt β2m (*16*, *17*). The W60G mutant shows a distinct behaviour also under denaturing conditions, where it shows kinetics of disulphide reduction slower than wt β2m. The crystal structure of the W60G mutant shows that all residues of the DE loop fall in the favoured regions of the Ramachandran plot, suggesting that the mutation to Gly confers higher overall stability to β2m, thanks to its unique conformational properties that help release stereochemical strain of the DE loop (*16*). Conversely, the mutation of Asp59 to Pro leads to a more strained DE loop, resulting in diminished thermal stability and increased propensity to form amyloid fibrils compared to wt β2m (*18*). Comparative analysis of the DE loop conformations shows that wt β2m and the D59P mutant display an irregular DE loop, while the W60G, W60V and W60C mutants host a regular β-turn (*19*). All such data suggest that increased stability of the DE loop may translate into β2m variants of increased overall stability. In this respect, we notice that the W60G mutant lacks a Pro residue in position 58 to reach the most favourite residue distribution for a type I β-turn in the DE loop (*20*).

Here, we report on the double substitution of β2m residues Lys58 with Pro and Trp60 with Gly. Our aim was to produce a β2m variant endowed with the most stable type I β-turn in the DE loop, and to analyse the effects of the double mutation on β2m overall properties. To this purpose, the isolated K58P-W60G mutant has been characterized by means of fluorescence, circular dichroism (CD), crystallography and mass spectrometry analyses. Furthermore, the K58P-W60G mutant amyloidogenic propensity was assessed at low and neutral pH values. The results here reported show that regularization of the protein conformation in the DE loop leads to stabilization of the whole β2m structure.

Materials and Methods

Mutagenesis, expression and purification

Mutagenesis of Lys58 to Pro was performed using the QuickChangeTM site-directed mutagenesis kit (Stratagene, La Jolla, CA, USA) starting from the plasmid of the W60G mutant (*16*). The following primers were used: for K58P, 5′-TCA GAC TTG TCT TTC AGC CCG GAC GGG TCT TTC TAT CTC TTG-3′ and 3′-CAA GAG ATA GAA AGA CCC GTC CGG GCT GAA AGA CAA GTC TGA-5′. The construct was introduced in the BL21-DE3 *Escherichia coli* strain. A methionine residue, present at the N-terminal position of all recombinant products, will be referred to as Met0. Expression and purification of wt and β2m K58P-W60G species were carried out as previously reported (*8*).

Thermal and chemical unfolding

In all the temperature ramps here described, β2m was in 50 mM sodium phosphate pH 7.4. The protein concentration was 1.4 mg/ml (cell path 1 cm) or 0.1 mg/ml (cell path 0.1 cm) for measurements in the near- and far-UV regions, respectively. The temperature increment was set to 50°C/h (0.83°C/min). β2m temperature unfolding from 20°C to 95°C has been simultaneously followed by intrinsic Trp fluorescence and by near-UV CD signals on a Jasco J-810 spectropolarimeter, equipped with a Peltier device and fluorescence detector. Wavelength was set at 293 nm to follow simultaneously the variation of molar ellipticity and to excite tryptophan. Emitted fluorescence was detected at 350 nm. The Trp-fluorescence of β2m variants bearing or not Trp60 is comparable since, as previously shown, the Trp60 fluorescence is almost totally quenched by the solvent (*21*). Temperature unfolding of β2m secondary structure has been monitored by far-UV CD at 202 nm.

Stopped-flow refolding

Kinetics of tertiary structure refolding was monitored by Trp-fluorescence for wt β2 microglobulin (β2m) and W60G β2m using a Bio-Logic SFM-300 stopped-flow fluorimeter, with an excitation wavelength of 295 nm and monitoring the total fluorescence emission change at 320 nm. All the experiments were performed at 303 K in 10 mM sodium phosphate buffer, pH 7.4, at 0.02 mg/ml final protein concentration. The refolding experiments were performed by a 10-fold dilution of unfolded protein samples (0.2 mg/ml in 4 M GdHCl).

Kinetics of the secondary structure recovery was studied by stopped-flow CD using a BioLogic SFM-20 stopped-flow system fitted to a Jasco J-810 spectropolarimeter. The protein (20 μl of 0.2 mg/ml in 4 M GdHCl) was mixed with 480 μl of buffer (sodium phosphate 50 mM pH 7.4) in 100 ms (dead time 10.8 ms). Data traces were recorded at 233 nm through a 2-mm cell path and fitted using a first-order rate equation by means of SigmaPlot 2001 software.

Crystallization and structure determination

The K58P-W60G β2m mutant was crystallized using the hanging-drop vapour diffusion technique under the following conditions: protein solution at a concentration of 10 mg/ml, sodium acetate 0.1 M pH 5.5, ammonium acetate 0.2 M, PEG4000 22%, glycerol 20%. Crystals of the mutant protein grew in few days at 20°C.

X-ray diffraction data were collected on flash-frozen crystals using the crystallization mother-liquor as cryoprotectant, at 100 K, at the beamline ID1-4 1 (the European Synchrotron Radiation Facility, ESRF, Grenoble, France). The K58P-W60G crystals diffracted to 1.25 Å resolution. Diffraction data were processed with MOSFLM (*22*) and SCALA (*23*). Phases were obtained by molecular replacement using MOLREP (*24*) and the W60G β2m mutant atomic coordinates (PDB code 2VB5) as search model. The refinement process was performed with REFMAC5, riding hydrogen atoms and anisotropic B factors have been applied at the end of the refinement (*25*). Model building, structure analysis and Kleywegt plot were carried out using COOT (*26*) (see Table II).

ESI–MS

A hybrid quadrupole-time-of-flight instrument (QSTAR Elite, Applied Biosystems, Foster City, CA, USA) was employed for ESI–MS analysis, using a nanospray source and metal-coated borosilicate capillaries with medium-length emitter tip of 1-μm internal diameter (Proxeon, Odense, Denmark). The following instrumental settings were applied: declustering potential 80 V; ion spray voltage 1.1–1.2 kV; curtain gas 20 PSI. Samples were sprayed at room temperature. Samples were prepared as equimolar mixtures of wt β2m and K58P-W60G mutant (5 μM each) in 10 mM ammonium acetate (Sigma Aldrich, St Louis, MO, USA), adjusting the pH to 7.4 or 2.5 with ammonium hydroxide (Sigma Aldrich, St Louis, MO, USA) or formic acid (Merck KGaA, Darmstadt, Germany), respectively.

Amyloid fibril formation at pH 7.4 and 2.5

β2m (100 μM) was incubated at 37°C in 50 mM phosphate buffer,100 mM NaCl, pH 7.4, in the presence of 20% (v/v) TFE (*7*). β2m fibril seeds (20 μg/ml) were added to the samples. To form amyloid fibrils at acidic pH, β2m (100 μM) was incubated at 37°C in 50 mM Na–citrate and 100 mM NaCl, pH 2.5, in the presence of 20 μg/ml of β2m fibril seeds (*27*). Quantification of amyloid formation was performed with ThT according to Ref. (*28*). ThT (SIGMA) concentration was 10 μM in 50 mM glycine–NaOH buffer, pH 8.5. A VARIAN Cary Eclipse spectrofluorimeter was used for the measurements, with excitation at 445 nm and emission collected at 480 nm, with slits set at 5 nm and high voltage. The measurements are the average of three independent experiments.

Results

Fold stability and folding kinetics

K58P-W60G β2m mutant conformational stability, determined by guanidium-hydrochloride equilibrium unfolding, shows an increased chemical stability with respect to wt β2m (melting concentration, $C_{m\ K58P\text{-}W60G} = 2.7$ M GdHCl versus $C_{m\ wt} = 1.7$ M GdHCl), while $\Delta G°(H_2O)$ is 7.6 kcal mol^{-1} for the K58P-W60G mutant and 5.5 kcal mol^{-1} for wt β2m; β2m chemical unfolding has been followed by Trp fluorescence (Fig. 1A). Furthermore, in order to obtain an independent assessment of the K58P-W60G β2m stability, thermal unfolding was monitored by CD (near- and far UV) (Fig. 1B) and by intrinsic fluorescence. Near-UV CD and Trp-fluorescence approaches show that the K58P-W60G β2m mutant displays distinctly higher tertiary structure stability relative to wt β2m, comparable to that achieved by the W60G mutant (Table I). Interestingly, far-UV CD analysis reveals that the K58P-W60G mutant has a melting temperature, $T_m = 73.5$°C, thus a thermal stability higher than both the W60G mutant and the wt protein ($T_{mW60G} = 69.8$°C and $T_{m\ wt} = 62.4$°C) (*17*) (Table I).

Refolding kinetics were monitored by intrinsic fluorescence (Fig. 2A and B). In the K58P-W60G mutant, the rate constant of the folding fast phase shifts from 1.6 s^{-1} for wt β2m to 10 s^{-1} for the mutant. The plateau is reached after 5 s for the mutant (versus 20 min required for wt β2m). Therefore, the slow phase of folding, observed for wt β2m, is not detectable in the double mutant, similarly to what has been previously reported for the W60G mutant (*16*).

In order to compare the folding process of wt β2m and the K58P-W60G β2m mutant based on secondary structure, refolding kinetics were monitored by CD at $\lambda = 233$ nm. As shown in Fig. 2C, the profiles for the two β2m variants are indistinguishable. It is noteworthy that the slow phase, which is observed in wt β2m folding by Trp-fluorescence, is absent in both wt and mutant β2m when refolding is monitored by far-UV CD.

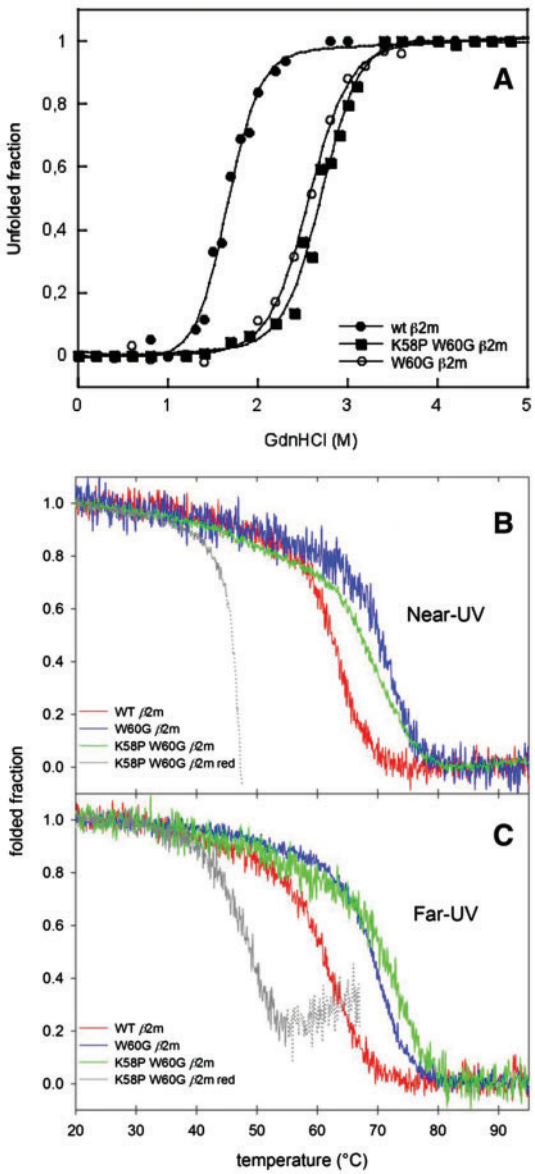

Fig. 1 Thermal and chemical fold stability of the K58P-W60G β2m mutant. (A) Unfolding titration curves as a function of denaturant (GdHCl) concentration for wt β2m, W60G and K58P-W60G mutants. The fraction of unfolded protein is reported on the *y*-axis. (B and C) Temperature dependence of circular dichroism signal, in near-UV (B) and far-UV (C) for w.t. β2m (red), K58P-W60G mutant (blue), reduced K58P-W60G (grey) and W60G mutant (green).

Crystal structure of K58P-W60G β2m mutant

The crystal structure of the K58P-W60G β2m mutant was solved and refined at 1.25 Å resolution, with R_{work} of 14.4% and R_{free} of 17.2% (Fig. 3A and Table II). All the 100 amino acids are clearly traced in the electron density, which is of excellent quality, clearly defining the mutated Pro58 and Gly60 residues. As for the other β2m mutants affecting residue 60 (*16*, *18*, *19*) in the K58P-W60G mutant the DE loop matches the

Table I. Summary of chemical and thermal unfolding results for β2m variants.

	Cm (GdHCl)	ΔG° (H_2O) kcal mol^{-1}	T_m (Near-UV) (°C)	T_m (Trp-fluorescence) (°C)	T_m (Far-UV) (°C)
wt β2m[a]	1.7 M	5.5	63.8	64.1	62.4
W60G mutant[a]	2.5 M	6.6	71.6	71.7	69.8
K58P-W60G mutant	2.7 M	7.6	69.9	73.0	73.5

[a]Melting temperatures taken from Santambrogio *et al.* (*17*).

canonical conformation of a type-I β turn. According to Hutchinson *et al.*, specific residues are preferred for each of the four positions of a type-I β turn, due to their stereochemical properties. At the β turn site *i* (corresponding to residue 57 in the K58P-W60G structure; Fig. 3B) a polar residue (typically Asp, Ser, Cys and His), which can establish a H-bond with the main chain nitrogen of the $i+2$ residue, is preferred. At site $i+1$, a Pro residue is favoured because of the restriction on the Φ angle to about -60°. At site $i+2$ Asp, Arg, Ser and Thr are preferred. Finally, at site $i+3$ Gly is the most favoured residue, since it helps the polypeptide chain return to an anti-parallel β-structure after completion of the turn (*20*). The K58P-W60G mutant, with its amino acid sequence 57-SPDG-60, thus displays the most favoured residues at each of the four sites. Moreover, residues Ser57 and Asp59, together with Ser61 (the first residue after the β turn), help stabilizing an overall compact structure in the 57–61 sequence stretch (Fig. 3B).

Relative to the other β2m mutants of known 3D structure, K58P-W60G shows a higher degree of alternative residue conformations. In particular, thanks the high resolution achieved, alternative conformations were observed for the aromatic residue cluster of Phe56 and Phe62. Moreover, the polypeptide backbone in the D strand was found in two similar but distinct conformations. Notably, the very high-resolution structure (1.13 Å) of wt β2m does not display any of such alternative conformations (*29*).

Unexpectedly, the disulphide bond between Cys25 and Cys80, which usually locks the two β2m β-sheets, was found severed in the crystal structure of the K58P-W60G mutant. To our knowledge, this is the first β2m structure where such a reduced disulphide bond is observed. Cys80 shows extra side chain density indicative of an oxidized species; the extra density was modelled as a sulphenic acid (i.e. −OH group bound to the thiol group; Fig. 3C). On the other side of the severed disulphide, Cys25 side chain is observed in three alternative conformations. The structures obtained from several crystals, grown from different purification batches, all show the same pattern of reduction. Given the known effects that X-rays may exert on proteins [reviewed in (*30*)], rupture of the disulphide bond can be (partly of fully) linked to the X-ray diffraction experiments run on a high-intensity synchrotron source. Nevertheless, the behaviour observed here, unprecedented for β2m, suggests that the disulphide bond in the K58P-W60G mutant is more labile to radiation damage than in wt and in the other previously described DE β2m mutants. However, radiation damage may be not the only factor, since several lines of evidence suggest that part of the protein is already reduced before crystallization (see below).

Unfolding and reduction monitored by ESI–MS

Figure 4 shows the nano-ESI–MS spectrum of an equimolar mixture of K58P-W60G mutant and wt β2m under non-denaturing conditions. The signals of the two proteins are clearly distinguishable due to their different masses. Both proteins are folded, as indicated by the narrow charge-state distribution (CSD) showing only the 8^+ and 7^+ ions. Mass deconvolution yields the values of $11{,}860 \pm 0.5$ Da for the wt protein, and $11{,}700 \pm 0.5$ Da for the mutant, in excellent agreement with the calculated mass for the proteins containing an oxidized disulphide (11,860.28 and 11,700.06 Da, respectively). By lowering the pH (Fig. 4B), the CSDs are shifted towards higher *z*-values, consistent with acid-induced protein denaturation taking place under such conditions. However, the main charge state of the wt protein is 11^+, while that of the mutant is 13^+, indicating more extensive unfolding in the latter. Interestingly, mass deconvolution performed only on the high-charge peaks of the mutant yields the mass of the disulphide-reduced protein ($11{,}702.06 \pm 0.5$ Da). These data indicate that part of the mutant protein is already in the reduced state in the absence of reducing agents. Such component is masked by the oxidized protein under mild ESI conditions, since both oxidized and reduced proteins populate the same charge states. However, it becomes detectable at low pH because protein unfolding can proceed more extensively in the reduced protein, leading to higher charge states than the unfolded protein with an intact disulphide. Thus, the highest charge state is dramatically enriched in the contribution of the reduced component and the 2-Da mass shift can be detected. No evidence of oxygen addition (i.e. formation of a sulphenic centre at Cys80) is found in the ESI–MS data, suggesting that the modification observed in the crystal structure is merely an artefact due to X-ray radiation damage.

Reduced K58P-W60G β2m mutant

Combining the information provided by crystallography and ESI–MS, we propose that in solution the K58P-W60G mutant may coexist as two species: the common disulphide-oxidized form and a reduced variant where the disulphide bond between Cys25 and Cys80 is absent. In order to verify such hypothesis, the K58P-W60G mutant protein was unfolded in 4 M GdHCl and the level of free cysteine was assessed by

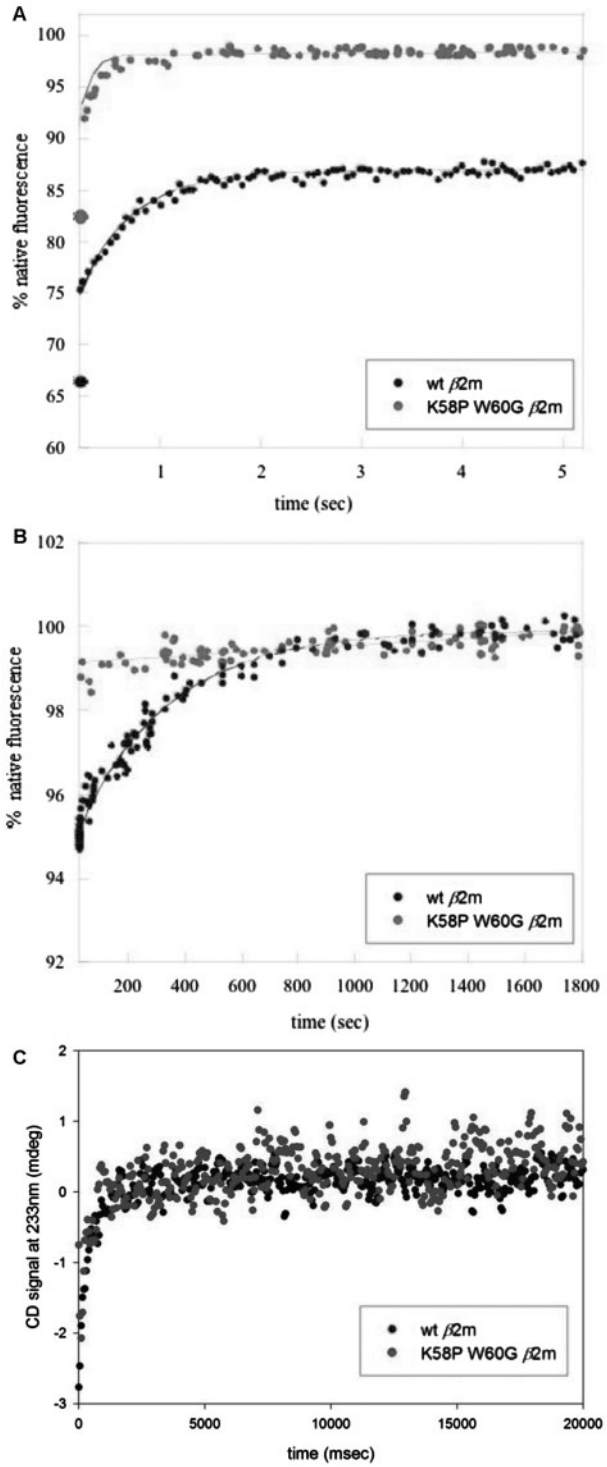

Fig. 2 Refolding kinetics of the K58P-W60G β2m mutant.
(A and B) Intrinsic fluorescence curves of wt β2m (black) and of the K58P-W60G mutant (grey), monitoring the fast-phase and the slow-phase of folding. (C) CD far-UV folding curves of wt β2m (black) and of the K58P-W60G mutant (grey).

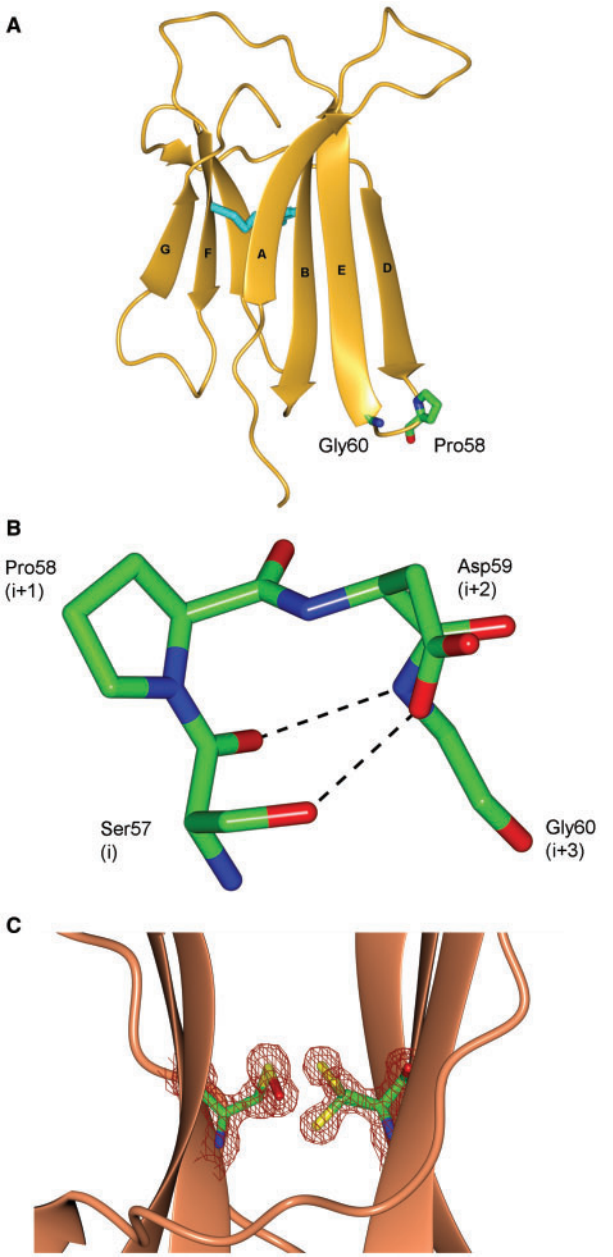

Fig. 3 Crystal structure of the K58P-W60G β2m mutant.
(A) Cartoon representation of the crystal structure of the K58P-W60G mutant. Strands are labelled according to the convention for β2m. Residues Cys25, Cys80 and the mutated Pro58 and Gly60 are shown as stick models. (B) Stick model of the K58P-W60G mutant DE loop. Residues are labelled according to Hutchinson *et al.* type I β-turn definition. H-bonds are shown by dotted lines; the H-bond linking Ser57 OG (i) and the peptidic N of Asp59 ($i+2$) is weak (3.43 Å) and has not been drawn. In addition to those shown in the figure, H-bonds ($\leq$3.0 Å) stabilizing the β-turn region are observed between: the peptidic N atom of Ser57 and the carbonyl O of Ser61 ($i+4$), Ser57 OG atom and the peptidic N of Ser61, the carboxylate of Asp59 and Ser61 OG. (C) The $2F_O - F_C$ electron density map of the severed disulphide bond in K58P-W60G, contoured at 1.0 σ, highlights the triple conformation of Cys25 and the oxidized Cys80 sulphenic centre (both represented as stick models).

titration with 5,5′-dithiobis-(2-nitrobenzoic acid) (DTNB). The titration confirmed that ~30% of the cysteines are in the reduced state (data not shown), indicating that in 30% of the β2m molecules present in solution the disulphide bond is severed. Subsequently, the ability of the reduced K58P-W60G mutant to fold to a wt-native structure was assessed. The mutant protein was unfolded and completely reduced by dithiothreitol (DTT) in the presence of GdHCl, and then refolded (by removal of GdHCl) in

the presence of DTT to prevent cysteine oxidation. The reduced K58P-W60G mutant was successfully refolded according to Ohhashi *et al.* (*31*) and the thermal stability of the reduced protein was monitored by CD (Fig. 1B). These observations are in keeping with previous results on the role of the disulphide bonds in immunoglobulin fold stability (*32*). A proper unfolding Tm could not be directly measured, since the reduced K58P-W60G mutant shows a distinct propensity to precipitate before the end of the transition (also at the low concentration used in the far-UV region). However, the onset of transition occurs at least 15–20°C lower than observed for the other mutants (Fig. 1B), allowing us to hypothesize that the T_m should fall below 50–55°C.

Intriguingly, a closer analysis of the thermal unfolding of the K58P-W60G mutant monitored by Trp-fluorescence revealed that the first derivative has a first, although minor, minimum at 48°C (Supplementary Fig. S1). This may well represent unfolding of the reduced K58P-W60G fraction (~30%). On the other hand, the temperature ramps monitored by near- and far-UV CD detect only the unfolding of a major protein component (i.e. the disulphide-oxidized form), due to the lower sensibility (signal-to-noise ratio) of the CD signal compared with Trp-fluorescence.

Table II. Data collection and refinement statistics for β2m K58P-W60G.

Beam line	ESRF ID14-1
Space group	Monoclinic C2
Unit cell constants (Å, °)	$a = 76.35$, $b = 28.58$, $c = 60.73$, $\beta = 132.9°$
Resolution (Å)	19.0–1.25 (1.32–1.25)
R_{merge}[a] (%)	10.0 (69.2)
$I/\sigma I$	15.5 (3.2)
Completeness (%)	99.6 (97.2)
Redundancy	10 (8.7)
Unique reflections	26776 (3812)
Refinement	
R_{work}[b] (%)	14.4
R_{free} (%)	17.2
Number of atoms	
Protein (Avg. B-factor, A^2)	935 (10.0)
Water (Avg. B-factor, A^2)	132 (21.0)
Ramachandran plot	
Most favoured region	99 (99%)
Allowed region	1 (1%)

Values in parentheses are for the highest resolution shell.
[a] $R_{merge} = \Sigma|I - \langle I \rangle|/\Sigma|I|$ where, I is the observed intensity and $\langle I \rangle$ is the average intensity.
[b] $R_{work} = \Sigma_{hkl}||F_o| - |F_c||/\Sigma_{hkl}|F_o|$ for all data except 5% which were used for R_{free} calculation.

Amyloid fibril formation

The K58P-W60G mutant propensity to form amyloid fibrils was analysed either at pH 7.4 in the presence of 20% TFE, or at pH 2.5, in both cases with small-controlled additions of wt β2m fibril seeds. Under both conditions, a wt β2m control fibrillogenesis was performed. The data at pH 7.4 show that, after 1 week of incubation at 37°C, wt β2m forms amyloid fibrils, bind thioflavin T (ThT) and is positive to Congo Red (CR) staining, while the K58P-W60G mutant does not bind ThT (Fig. 5) and displays a negative CR assay (data not shown). On the contrary, at pH 2.5, both wt β2m and the K58P-W60G mutant are prone to aggregation, as shown by ThT and CR assays, with a higher fibril yield for the K58P-W60G mutant relative to wt β2m. Such distinct behaviour is similar to what has been observed for the W60G β2m mutant (*16*).

Discussion

Recent studies have focused the attention on the crucial role(s) played by Pro residues on β2m fold and stability. The Pro5 to Gly mutation results in the accumulation of an amyloidogenic intermediate with

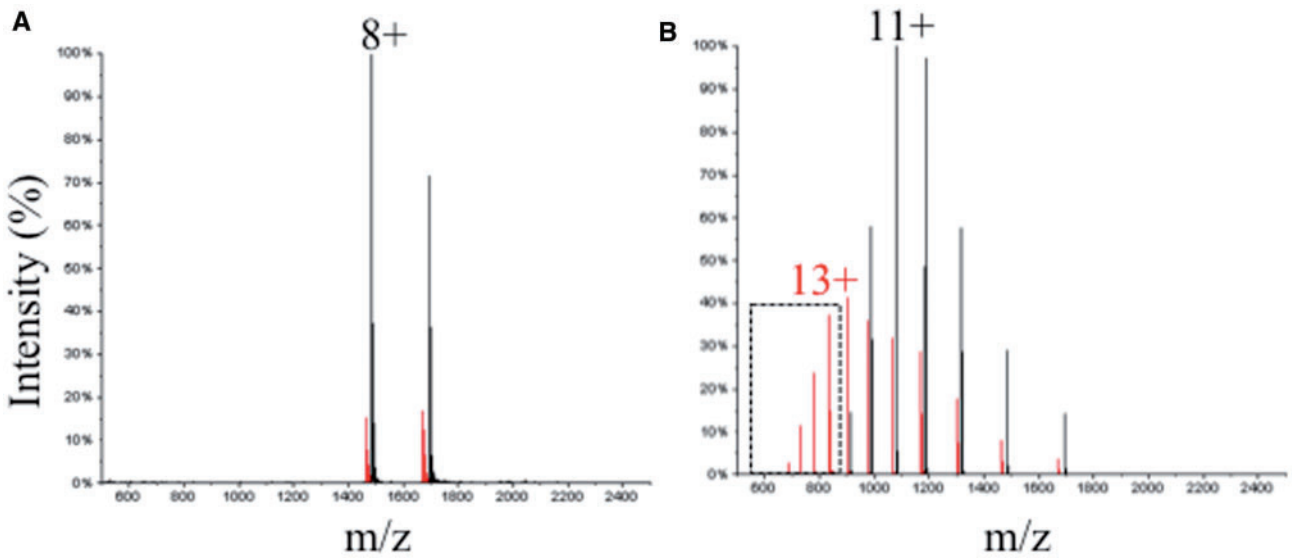

Fig. 4 Fold stability of reduced and oxidized K58P-W60G β2m mutant monitored by ESI-MS. Nano-ESI–MS spectra of an equimolar (5 μM) mixture of wt β2m (black) and K58P-W60G mutant (red) in 10 mM ammonium acetate, pH 7.4 (A) or pH 2.5 (B). The instrument interface was set at room temperature. The most intense charge state of each component is labelled by the corresponding charge state. Peaks in the dashed boxes correspond to the fully reduced mutant protein (11 702 Da).

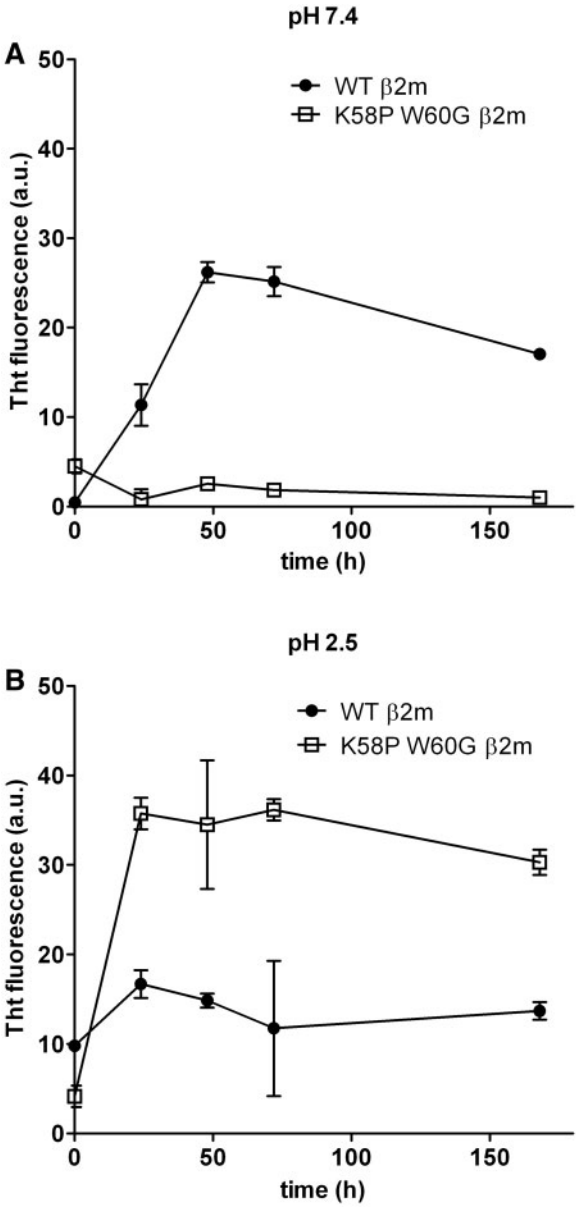

Fig. 5 Kinetics of fibril formation for wt β2m and for K58P-W60G mutant, at pH 7.4 and pH 2.5, monitored by fluorescence using ThT binding assay. Wt β2m and K58P-W60G were incubated at 37°C and diluted to 100 μM concentration in a buffer containing 50 mM Na phosphate and 100 mM NaCl, pH 7.4 in the presence of 20% TFE (v/v) and 2.5 μg/ml wt β2m fibril seeds. wt β2m and K58P-W60G were incubated at 37°C and diluted to a final 100 μM concentration in a buffer containing Na–citrate 50 and 100 mM NaCl, pH 2.5 in the presence of 2.5 μg/ml wt β2m fibril seeds.

lower structural compactness than observed for the native protein, causing a higher propensity to aggregate for the P5G mutant than for wt β2m (*9*). Mutations of Pro32 also lead to β2m variants with non-native fold and with different amyloidogenic properties compared with the wt protein (*10*, *33*, *34*). Both Pro5 and Pro32 are located in loops, where they likely help holding the entire protein in the compact native fold. On the other hand, we have recently prepared a β2m DE loop mutant introducing a Pro residue in position 59 (*18*). The presence of a proline in the DE loop does not affect the overall protein fold, however it increases the loop geometrical strain, lowering β2m fold stability and markedly enhancing its amyloidogenic propensity (*17*, *18*). These three examples show how 'native Pro' residues are carefully located in order to increase the stability of loops, and, in general, of the β-sandwich structure, while not adding strain to β2m backbone geometry.

In a recent work, the Trp60 to Gly mutation was shown to give rise to a regular β-turn conformation in the DE loop region (*16*). The work reported here introduced the Lys58 to Pro mutation (in addition to the Trp60 to Gly mutation) in order to mimic the effect of a 'native Pro' residue, e.g. to serve as a 'lock' of a loop, and to stabilize the overall protein conformation by building an ideal type-I β-turn. Complementary biophysical and structural techniques have been used to characterize the double mutant. As a first result, we confirm that the DE loop indeed adopts the ideal type I β-turn conformation (Fig. 3B), with Pro58 occupying position $i+1$ of the turn. Thermal and chemical unfolding indicates that the K58P-W60G mutant has a distinctly higher conformational stability than wt β2m (Fig. 1). Folding experiments show that the K58P-W60G mutant folds faster than the wt protein, and that the folding slow phase is absent (Fig. 2). Additionally, the double mutation leads to a variant that does not form amyloid under the standard conditions at pH 7.4 with 20% TFE.

The comparison between the K58P-W60G and the W60G mutant shows subtle yet interesting differences. The K58P-W60G mutant displays fold stability, as well as folding kinetics, comparable to the W60G mutant [this work and (*16*)], and the two protein structures are virtually identical (0.34 Å r.m.s.d. over 99 Cα pairs). The K58P-W60G and the W60G mutants display very similar propensities towards amyloid aggregation. However, an unexpected difference is that while the W60G mutant, as all other β2m variants characterized to date, shows a completely oxidized (intact) Cys25–Cys80 disulphide, the purified K58P-W60G mutant is a mixture of oxidized (~70%) and reduced (~30%) molecules, the latter lacking the stabilizing effects of the disulphide. Notably, in the K58P-W60G mutant crystal structure the disulphide bond is fully severed. Considering that no structural changes appear to affect the protein backbone of the mutant, thus its protein packing capability in the crystal lattice, likely both oxidized and reduced forms coexist in the crystals, even before exposure to X-rays. Complete rupture of the disulphide bond is an effect of radiation damage that is particularly visible in the case of the K58P-W60G mutant. Indeed ESI–MS analysis, DTNB titrations and protein unfolding monitored by Trp-fluorescence (Fig. 4 and Supplementary Fig. S1) show that a sizeable fraction of the purified protein is reduced, lacking an intact disulphide bond. Such an observation would be in keeping with a peculiar behaviour occasionally observed at the end of the mutant protein purification, whereby the purified K58P-W60G mutant formed an ensemble of SDS-resistant oligomers, which may correspond to covalent association of β2m molecules through intermolecular disulphide bonds (Supplementary Fig. S2B).

In our laboratory all β2m mutants are purified under denaturing conditions and subsequently refolded according to a standard protocol (*8*). After the refolding step, ion exchange chromatography is used to separate the protein population endowed with the correct surface charges (i.e. properly folded). It is also known that the disulphide bond is crucial for β2m to achieve a correct fold, and is formed in the fast-phase of the folding. Indeed, in our hands all the previously purified β2m variants displayed an oxidized disulphide, suggesting that the disulphide-reduced molecules either fail the refolding step or are discarded through the ion exchange chromatography step. Interestingly, while all β2m variants show some precipitate during the folding procedure (often the amount of precipitate relates to the variant stability), upon refolding of the K58P-W60G mutant almost no precipitate has been observed, suggesting that the K58P-W60G mutant may have a remarkable folding efficiency and that the disulphide-reduced form that achieves a proper fold can efficiently mimic the native oxidized variant. The disulphide-reduced K58P-W60G β2m mutant molecules are soluble and stable in solution, can crystallize, and do not display higher aggregation forms in size exclusion chromatography (data not shown). Such a novel behaviour may be related to stabilization encoded by the DE loop mutations, being specific for the K58P-W60G mutant and distinct from the W60G mutant, where disulphide-reduced properly folded molecules have not been observed.

Previously characterized β2m mutants show that modifying the DE loop backbone geometry deeply affects β2m stability and amyloid propensity (*16–19*). The evidences here reported additionally stress the structural role of the DE loop in β2m folding and stability; particularly, in the case of the K58P-W60G double mutation, the DE loop properties appear to affect not only fold stability but also the folding pathway. In apparent contrast with what has been reported for wt β2m, in the K58P-W60G mutant the disulphide bond is not as crucial for β2m folding, and the DE loop can promote folding independently of the disulphide bond redox state.

Supplementary Data

Supplementary Data are available at *JB* Online.

Acknowledgements

We are grateful to Prof. G. Merlini (IRCCS Policlinico San Matteo, Pavia, Italy) for helpful discussion and continuous support.

Funding

Fondazione Cariplo, Milano, Italy (N.O.B.E.L. Project: Transcriptomics and Proteomics Approaches to Diseases of High Sociomedical Impact: A Technology Integrated Network), from the Italian MIUR (FIRB contract RBLA03B3KC_005), from the EU grant EURAMY, by FAR (Fondo Ateneo per la Ricerca) to R.G.

Conflict of interest

None declared.

References

1. Merlini, G. and Bellotti, V. (2003) Molecular mechanisms of amyloidosis. *N. Engl. J. Med.* **349**, 583–596
2. Sunde, M., Serpell, L.C., Bartlam, M., Fraser, P.E., Pepys, M.B., and Blake, C.C. (1997) Common core structure of amyloid fibrils by synchrotron X-ray diffraction. *J. Mol. Biol.* **273**, 729–739
3. Kad, N.M., Myers, S.L., Smith, D.P., Smith, D.A., Radford, S.E., and Thomson, N.H. (2003) Hierarchical assembly of beta2-microglobulin amyloid in vitro revealed by atomic force microscopy. *J. Mol. Biol.* **330**, 785–797
4. Porcelli, S.A. and Modlin, R.L. (1999) The CD1 system: antigen-presenting molecules for T cell recognition of lipids and glycolipids. *Annu. Rev. Immunol.* **17**, 297–329
5. Floege, J. and Ketteler, M. (2001) beta2-microglobulin-derived amyloidosis: an update. *Kidney Int. Suppl.* **78**, S164–S171
6. Gejyo, F., Yamada, T., Odani, S., Nakagawa, Y., Arakawa, M., Kunitomo, T., Kataoka, H., Suzuki, M., Hirasawa, Y., Shirahama, T., Cohen, A.S., and Schimd, K. (1985) A new form of amyloid protein associated with chronic hemodialysis was identified as beta 2-microglobulin. *Biochem. Biophys. Res. Commun.* **129**, 701–706
7. Yamamoto, S., Yamaguchi, I., Hasegawa, K., Tsutsumi, S., Goto, Y., Gejyo, F., and Naiki, H. (2004) Glycosaminoglycans enhance the trifluoroethanol-induced extension of beta 2-microglobulin-related amyloid fibrils at a neutral pH. *J. Am. Soc. Nephrol.* **15**, 126–133
8. Esposito, G., Michelutti, R., Verdone, G., Viglino, P., Hernandez, H., Robinson, C.V., Amoresano, A., Dal Piaz, F., Monti, M., Pucci, P., Mangione, P., Stoppini, M., Merlini, G., Ferri, G., and Bellotti, V. (2000) Removal of the N-terminal hexapeptide from human beta2-microglobulin facilitates protein aggregation and fibril formation. *Protein Sci.* **9**, 831–845
9. Eichner, T. and Radford, S.E. (2009) A generic mechanism of beta2-microglobulin amyloid assembly at neutral pH involving a specific proline switch. *J. Mol. Biol.* **386**, 1312–1326
10. Eakin, C.M., Berman, A.J., and Miranker, A.D. (2006) A native to amyloidogenic transition regulated by a backbone trigger. *Nat. Struct. Mol. Biol.* **13**, 202–208
11. Platt, G.W., Routledge, K.E., Homans, S.W., and Radford, S.E. (2008) Fibril growth kinetics reveal a region of beta2-microglobulin important for nucleation and elongation of aggregation. *J. Mol. Biol.* **378**, 251–263
12. Borysik, A.J., Radford, S.E., and Ashcroft, A.E. (2004) Co-populated conformational ensembles of beta2-microglobulin uncovered quantitatively by electrospray ionization mass spectrometry. *J. Biol. Chem.* **279**, 27069–27077
13. Mendoza, V.L., Antwi, K., Baron-Rodriguez, M.A., Blanco, C., and Vachet, R.W. (2010) Structure of the preamyloid dimer of beta-2-microglobulin from covalent labeling and mass spectrometry. *Biochemistry* **49**, 1522–1532
14. Smith, D.P., Giles, K., Bateman, R.H., Radford, S.E., and Ashcroft, A.E. (2007) Monitoring copopulated conformational states during protein folding events using electrospray ionization-ion mobility spectrometry-mass spectrometry. *J. Am. Soc. Mass Spectrom.* **18**, 2180–2190
15. Smith, D.P., Radford, S.E., and Ashcroft, A.E. (2010) Elongated oligomers in beta2-microglobulin amyloid

assembly revealed by ion mobility spectrometry-mass spectrometry. *Proc. Natl. Acad. Sci. USA* **107**, 6794–6798
16. Esposito, G., Ricagno, S., Corazza, A., Rennella, E., Gumral, D., Mimmi, M.C., Betto, E., Pucillo, C.E., Fogolari, F., Viglino, P., Raimondi, S., Giorgetti, S., Bolognesi, B., Merlini, G., Stoppini, M., Bolognesi, M., and Bellotti, V. (2008) The controlling roles of Trp60 and Trp95 in beta2-microglobulin function, folding and amyloid aggregation properties. *J. Mol. Biol.* **378**, 885–895
17. Santambrogio, C., Ricagno, S., Colombo, M., Barbiroli, A., Bonomi, F., Bellotti, V., Bolognesi, M., and Grandori, R. (2010) DE-loop mutations affect beta2 microglobulin stability, oligomerization, and the low-pH unfolded form. *Protein Sci.* **19**, 1386–1394
18. Ricagno, S., Colombo, M., de Rosa, M., Sangiovanni, E., Giorgetti, S., Raimondi, S., Bellotti, V., and Bolognesi, M. (2008) DE loop mutations affect beta-2 microglobulin stability and amyloid aggregation. *Biochem. Biophys. Res. Commun.* **377**, 146–150
19. Ricagno, S., Raimondi, S., Giorgetti, S., Bellotti, V., and Bolognesi, M. (2009) Human beta-2 microglobulin W60V mutant structure: Implications for stability and amyloid aggregation. *Biochem. Biophys. Res. Commun.* **380**, 543–547
20. Hutchinson, E.G. and Thornton, J.M. (1994) A revised set of potentials for beta-turn formation in proteins. *Protein Sci.* **3**, 2207–2216
21. Kihara, M., Chatani, E., Iwata, K., Yamamoto, K., Matsuura, T., Nakagawa, A., Naiki, H., and Goto, Y. (2006) Conformation of amyloid fibrils of beta2-microglobulin probed by tryptophan mutagenesis. *J. Biol. Chem.* **281**, 31061–31069
22. Leslie, A.G.W. (1992) Recent changes to the MOSFLM package for processing film and image plate data. *Joint CCP4 + ESF-EACMB Newsletter on Protein Crystallography*
23. CCP4. (1994) The CCP4 suite: programs for protein crystallography. *Acta Crystallogr.* **50**, 760–763
24. Vagin, A.A. and Teplyakov, A. (1997) MOLREP: an automated program for molecular replacement. *J. Appl. Crystallogr.* **30**, 1022–1025
25. Murshudov, G.N., Vagin, A.A., and Dodson, E.J. (1997) Refinement of macromolecular structures by the maximum-likelihood method. *Acta Crystallogr.* **53**, 240–255
26. Emsley, P. and Cowtan, K. (2004) Coot: model-building tools for molecular graphics. *Acta Crystallogr.* **60**, 2126–2132
27. Naiki, H., Haschimoto, N., Suzuki, S., Rimura, H., Nakakuki, K., and Gejyo, F. (1997) Establishment of a kinetic model of dialysis-related amyloid fibril extension in vitro. *AMYLOID: Int. Exp. Clin. Invest.* **4**, 223–232
28. LeVine, H. III (1993) Thioflavine T interaction with synthetic Alzheimer's disease beta-amyloid peptides: detection of amyloid aggregation in solution. *Protein Sci.* **2**, 404–410
29. Iwata, K., Matsuura, T., Sakurai, K., Nakagawa, A., and Goto, Y. (2007) High-resolution Crystal Structure of beta2-Microglobulin Formed at pH 7.0. *J. Biochem.* **142**, 413–419
30. Garman, E.F. (2010) Radiation damage in macromolecular crystallography: what is it and why should we care? *Acta Crystallogr.* **66**, 339–351
31. Ohhashi, Y., Hagihara, Y., Kozhukh, G., Hoshino, M., Hasegawa, K., Yamaguchi, I., Naiki, H., and Goto, Y. (2002) The intrachain disulfide bond of beta(2)-microglobulin is not essential for the immunoglobulin fold at neutral pH, but is essential for amyloid fibril formation at acidic pH. *J. Biochem.* **131**, 45–52
32. Goto, Y. and Hamaguchi, K. (1979) The role of the intrachain disulfide bond in the conformation and stability of the constant fragment of the immunoglobulin light chain. *J. Biochem.* **86**, 1433–1441
33. Jahn, T.R., Parker, M.J., Homans, S.W., and Radford, S.E. (2006) Amyloid formation under physiological conditions proceeds via a native-like folding intermediate. *Nat. Struct. Mol. Biol.* **13**, 195–201
34. Sakata, M., Chatani, E., Kameda, A., Sakurai, K., Naiki, H., and Goto, Y. (2008) Kinetic coupling of folding and prolyl isomerization of beta2-microglobulin studied by mutational analysis. *J. Mol. Biol.* **382**, 1242–1255